



HAL
open science

Thermal transfer in Rayleigh-Bénard convection with and without roughness elements

Éléonore Rusaouen, Olivier Liot, Bernard Castaing, Julien Salort, Francesca
Chillà

► **To cite this version:**

Éléonore Rusaouen, Olivier Liot, Bernard Castaing, Julien Salort, Francesca Chillà. Thermal transfer in Rayleigh-Bénard convection with and without roughness elements. 2017. hal-01508393v1

HAL Id: hal-01508393

<https://hal.science/hal-01508393v1>

Preprint submitted on 14 Apr 2017 (v1), last revised 21 Sep 2017 (v2)

HAL is a multi-disciplinary open access archive for the deposit and dissemination of scientific research documents, whether they are published or not. The documents may come from teaching and research institutions in France or abroad, or from public or private research centers.

L'archive ouverte pluridisciplinaire **HAL**, est destinée au dépôt et à la diffusion de documents scientifiques de niveau recherche, publiés ou non, émanant des établissements d'enseignement et de recherche français ou étrangers, des laboratoires publics ou privés.

Thermal transfer in Rayleigh-Bénard convection with and without roughness elements

E.Rusaouen^{1*}, O. Liot^{1†}, B. Castaing², J.Salort¹, F. Chillà¹

December 2016

¹Univ Lyon, Ens de Lyon, Univ Claude Bernard, CNRS, Laboratoire de Physique, F-69342 Lyon, France

²Univ. Grenoble Alpes, CNRS, Grenoble INP, LEGI, F-38000 Grenoble, France

Abstract

Several Rayleigh-Bénard experiments in water are performed with and without roughness elements. We present new thermal transfer measurements obtained with large roughness elements arranged in a square lattice. The data are compared to previous ones obtained using smaller elements in the same cell. Experiments in the same apparatus without roughness are presented, as reference results in order to allow for comparison. Several regimes of heat transfer, in the rough case, are identified : a regime similar to the smooth case, an enhanced heat transfer one characterized by a modification of the Nusselt vs Rayleigh numbers relation, and a saturation part where the relation can be similar to a smooth one with a corrected prefactor.

1 Introduction

Turbulent Rayleigh-Bénard convection is a model system for natural convection. Theoretically, it consists in a horizontal infinite fluid layer inserted between two plates: a hot at the bottom and a cold one at the top. The difference of temperature ΔT between the two plates induces a fluid flow. It is characterized by the Rayleigh number,

$$Ra = \frac{\alpha \Delta T g H^3}{(\nu \kappa)}, \quad (1)$$

where H is the distance between the two plates, α is the expansion coefficient of the fluid, ν its kinematic viscosity, κ the thermal diffusivity and g the acceleration due to gravity. The system response is the Nusselt number,

$$Nu = \frac{QH}{(\lambda \Delta T)}, \quad (2)$$

where λ is the thermal conduction and Q the thermal flux through the fluid. This Nusselt number corresponds to the balance of the thermal transfer with the corresponding conductive one at a given difference of temperature. It is then a measurement of the efficiency of the thermal transfer versus the equivalent purely conductive one. In the present paper, this ratio is the efficiency of convection versus equivalent conduction. The fluid properties are characterized using the Prandtl number, which balances the kinematic viscosity to the thermal diffusivity,

$$Pr = \frac{\nu}{\kappa}. \quad (3)$$

In laboratory the corresponding experiment is the Rayleigh-Bénard cell where the layer of fluid is not infinite but confined into a tank. The cell is geometrically defined by its vertical aspect ratio $\Gamma = D/H$, where D is, here, the diameter of the cell, and H its height. It represents the confinement of the fluid in the experiment. One possibility to describe the turbulent thermal behavior of a cell is the use of a power law relating the Nusselt number to the Rayleigh and Prandtl numbers,

$$Nu = C Ra^a Pr^b. \quad (4)$$

*presently at Univ. Grenoble Alpes, CNRS, Grenoble INP, LEGI, F-38000 Grenoble, France.

†presently at LAAS-CNRS, 7 avenue du Colonel Roche, BP54200 31031 Toulouse Cedex 4, France.

In order to explore a possible perturbation of the boundary layers, and then a modification of thermal transfer of cells, experiments involving roughness had been performed. Roughness elements can be added on only one of the horizontal plates, S. Ciliberto [1999], J.-C. Tisserand [2011] or P. Wei [2014], or on both plates, Y.-B. Du [1998] and Y.-B. Du [2000] or X.-L. Qiu [2005], or even on the entire cell, P.-E. Roche [2001a]. Several geometries of structure are used such as square pyramids, Y.-B. Du [1998], Y.-B. Du [2000] for example, pyramidal grooves, P.-E. Roche [2001a], spheres S. Ciliberto [1999] or square structures J.-C. Tisserand [2011]. Those experiments can be separated into two classes: the ones using non-conductive roughness elements added to a smooth plate, S. Ciliberto [1999], the second class groups experiments performed using conductive roughness, J.-C. Tisserand [2011] or P. Wei [2014]. This second group exhibits some common properties. Two of them are now well-established: thermally conductive roughness induces an enhancement of the thermal transfer through the cell, and this enhancement appears when the height of the thermal boundary layer, noted δ_θ , reaches the height of the roughness, noted h_0 , whatever the shape of the structure used.

The general behavior comes with other properties which are not always observed. This can create an apparent discrepancy between different experiments. J.-C. Tisserand [2011], P.-E. Roche [2001a], X.-L. Qiu [2005] and in certain configuration P. Wei [2014] observe an increase of the power law exponent a . Before the transition to Nusselt enhancement, a is close to $2/7$ or $1/3$ whereas after it increases and reaches nearly $1/2$. Other results suggest that the exponent a can be unchanged but the prefactor \mathcal{C} may increase significantly, Y.-B. Du [1998] or P. Wei [2014] in other configurations.

After description of the experimental apparatus, section 2, we will detail some reference results obtained in the classical smooth configuration of the cell, section 3. Then, following the previous study of J.-C. Tisserand [2011], we will present results obtained in the rough cell with larger roughness elements, section 4. Structures are machined on the hot bottom plate and the cold plate is kept smooth. This allows us to explore the thermal behavior of the cell when the height of the thermal boundary layer is significantly smaller than the height of the elements. In the following part, 5, we shall compare our data to others obtained with pyramids and using this large corpus of data, we will try to extract general properties of thermally conductive roughness elements, before conclusion in section 6.

2 Experimental apparatus

2.1 The cell

The experimental apparatus consists in a cylinder, sketched in figure 1. As we use two different lateral walls, the cell can exhibit two aspect ratios Γ . Figure 1 sketches the aspect ratio $1/2$ which corresponds to a 1 m high cylinder. The diameter D is 0.5 m. We will call this configuration 'Large Cell' (\mathcal{LC}). The other aspect ratio corresponds to a 0.2 m high cylinder of the same diameter. The aspect ratio is then $\Gamma = 2.5$. We will call this configuration 'Small Cell' (\mathcal{SC}). The lateral walls are in stainless steel and their thickness is 3 mm.

The cold plate is in copper coated with a thin layer of nickel in order to prevent chemical attack from the working fluid, here deionised and degased water. It is regulated by a water circulation on its top. The circulation is controlled by a regulated bath. The hot plate, is made of aluminum. It is heated by Joule effect using a spiralled resistor of 13Ω inserted into the plate. The roughness is machined directly into the plate to preserve the physical properties of the material. Figure 2 sketches the roughness pattern used. In the present case, $h_0 = 4$ mm and $d = 10$ mm. The periodicity of the pattern is $2d$. J.-C. Tisserand [2011] used elements with $h_0 = 2$ mm and $d = 5$ mm arranged in the same way.

The cell is covered by a thermal insulator, a neopren foam, 4 cm thick, and enclosed into a thermal screen in copper. The mean temperature of the screen is regulated at the bulk temperature by a water bath in order to prevent interaction between the cell and the environnement. The entire apparatus is placed on a table whose temperature is also regulated at the bulk temperature.

2.2 Measurement techniques

Measurements are focused on thermal transfer. To do so, the cell is instrumented with different kinds of thermometers. Six thermistors Pt100, three per plates, measure the absolute value of the temperature of the plate. Six thermocouple junctions measure the temperature at mid height and the temperature of the bottom plate relative to the top plate with high accuracy. The common reference is then inserted into the cold plate which provides the relative zero value in the system, noted T_c . Another junction is also introduced into this plate at a different radius. Two junctions are placed into the hot plate, and provide the hot temperature T_h . As the thin lateral walls are in stainless steel, they are thermalized at the same temperature as the bulk flow. Two junctions are placed onto those

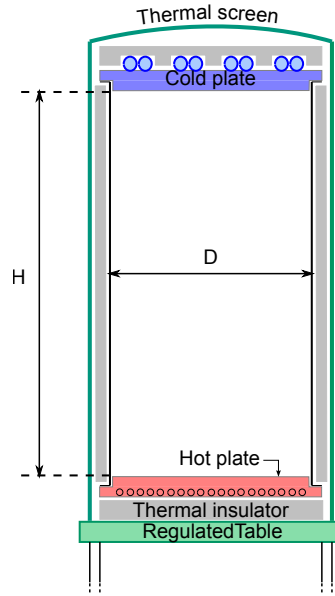


Figure 1: Sketch of the $\Gamma = 1/2$ Rayleigh-Bénard cell. Two aspect ratio can be used : $\Gamma = 1/2$ corresponding to a diameter $D = 50$ cm and a height $H = 1$ m, and $\Gamma = 2.5$ with $D = 50$ cm and $H = 20$ cm.

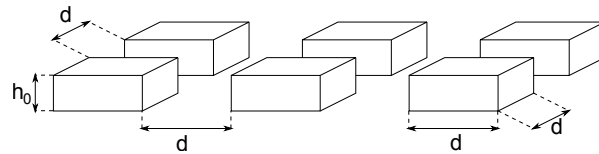


Figure 2: Sketch of the roughness pattern. In the present paper, results are obtained using $h_0 = 4$ mm, $d = 10$ mm with a periodicity $2d = 5h_0$. In J.-C. Tisserand [2011], $h_0 = 2$ mm and $d = 5$ mm.

walls to access the bulk temperature T_b . We also measure the temperature of the thermal screen and of the table. The thermocouple junctions are connected to an electronic amplifier without offset. The signal is amplified 2000 times. One mean point consists in several hours (typically 48 h) of recording.

By varying the bulk temperature of the fluid, we induce variations of the fluid properties resulting in variations of the Prandtl number. Keeping this bulk temperature constant in a serie of measurements groups results in series at constant Prandtl number. This allows us to check the potential influence of the Prandtl number in a range of values between 2.5 and 6.5.

2.3 Non-Boussinesq and lateral walls corrections

Since our experimental procedure is the same as the one used by J.-C. Tisserand [2011], we will use similar corrections which are reminded below. First, we take care of the Non-Boussinesq (NOB) effects. Indeed, under the Boussinesq approximation, we assume that all the physical properties of the fluid are independent of the temperature except the density ρ in the buoyancy term, which can be approximated as $\rho = \rho_0(1 - \alpha\Delta T)$, where ρ_0 is the density of water at the temperature T_b . Experiments performed by G. Ahlers [2006] suggest that the main effect of NOB effects on the Nusselt number comes from the variation of kinematic viscosity ν and thermal diffusivity κ only. In liquid water, the second one is nearly constant. The only remaining source of troubles is ν . They define parameter χ corresponding to this influence.

$$\chi = \frac{T_h - T_b}{T_b - T_c} = 1 - c_2\Delta T \quad (5)$$

J.-C. Tisserand [2011] used a logarithmic dependence of c_2 in Prandtl number but no dependence in Rayleigh number.

$$c_2 = -0.061Pr^{0.25} \frac{d\ln(\nu)}{dT} \quad (6)$$

This results in corrective prefactors on the Nusselt number such as $Nu_s^{cor} = (1 + c_2\Delta T_s/2)Nu_s$. The deviation remains smaller than 1% in all our experimental conditions, and thus can be neglected.

The second effect we have to consider is the spurious heat conduction in the walls, P.-E. Roche [2001b] and Ahlers [2000]. The thermal conductivity of the side walls has to be taken into account. It behaves as if the effective surface, S_{eff} , of the horizontal plates is larger than the real one S . They are related by $S_{eff} = (1 + f(W))S$, where W balances the heat conductivity of the side walls to the water one and is close to 0.5, and the corrected Nusselt number is

$$Nu^{cor} = Nu^{raw}(1 + f(W))^{-1}. \quad (7)$$

It yields to corrective prefactors. Figure 3 shows the typical values obtained for a smooth plate. The corrections for the rough plate are expressed in J.-C. Tisserand [2011], and we shall use the same here.

3 Reference smooth cell

Before consideration on results obtained using roughness, we shall discuss the behavior of \mathcal{LC} when using only smooth plates. Indeed, those results were briefly discussed only in the review F. Chillà [2012], but no detailed presentation is available in litterature.

The experimental apparatus is the same as the one described in section 2. The plates are both smooth, made of copper and coated with a thin layer of nickel. The results are presented in figures 4(a) and 4(b). Figure 4(a) shows the Nusselt number compensated by the Rayleigh number

$$\frac{Nu}{Ra^{1/3}}. \quad (8)$$

The \mathcal{LC} points are shown as full black diamonds in this figure. This presentation allows to evaluate the potential departure from a $Ra^{1/3}$ behavior. Other results obtained in other cells are also shown for comparison. The open triangles are for X. Chavanne [2001], a cylindrical cell of gaseous cryogenic helium. Green open diamonds and half-diamonds are for J.J. Niemela [2000], in a second cylindrical cell filled with gaseous helium. Violet crosses and circles are for the smooth/smooth values of Y.-B. Du [2000], in cylindrical cell filled with water at ambient temperature. Finally, blue stars are for P. Urban [2011], in a third cylindrical cell filled with gaseous cryogenic helium. The black line is the Grossmann-Lohse model fitted for $Pr = 3.7$. This model was first presented by S. Grossmann

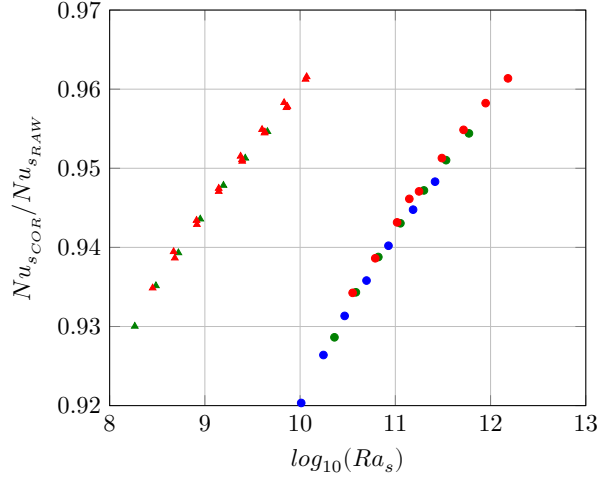


Figure 3: Corrective prefactors induced by side walls effects for a smooth plate (for more details on the definitions of Nu_s and Ra_s see expressions 11). Circles are for \mathcal{LC} cell and triangles are for \mathcal{SC} . Red refers to series at mean temperature 60°C , green is for 40°C and blue for 30°C .

[2000] to interpret the thermal transfer results of several Rayleigh-Bénard cells. The present evaluation of Nu_{GL} is performed using the updated prefactors of the GL-model proposed by R. J. A. M. Stevens [2013], as it will be in the entire paper. This model fairly represents the general behavior of all Rayleigh-Bénard cells in the present Rayleigh number range. Comparison with other experiments also shows a global collapse of all the cells. Note that some points from the Chavanne's experiment exhibit a departure from other experiments at $Ra > 1.10^{11}$. The present experiment does not exhibit such a departure even at similar Prandtl number.

Figure 4(b) shows the same experiment in a (Ra, Pr) phase diagram. Note that several points of the \mathcal{LC} experiment do not overlap with previous measurements in this (Ra, Pr) plane. Even if other experiments had been performed and are not presented here, to our knowledge, the \mathcal{LC} data are the only ones which range from $Ra = 1.10^{10}$ to $Ra = 1.10^{11}$ and $Pr > 6$. The corresponding values of Nusselt, Rayleigh and Prandtl numbers of those points are given in table 3.

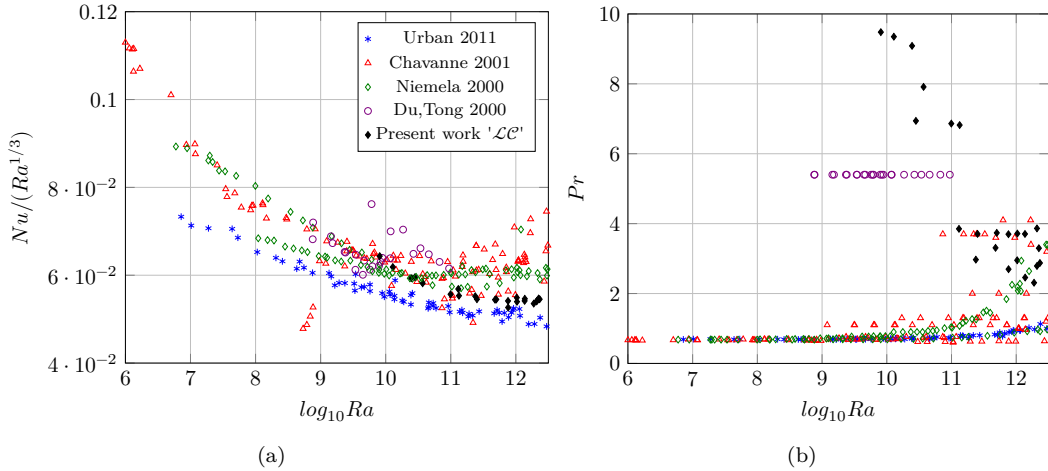


Figure 4: (a) : compensated Nusselt number as a function of the Rayleigh number. The symbols are the same as in figure 4(b). The continuous black line is the Grossmann-Lohse model with $Pr = 3.7$. The present points are represented by the full black diamond. (b) : Prandtl number as a function of Rayleigh number.

Pr	Ra	Nu	Pr	Ra	Nu
9.48	$8.10 \cdot 10^9$	129	2.97	$1.37 \cdot 10^{12}$	601
9.35	$1.27 \cdot 10^{10}$	145	3.31	$1.04 \cdot 10^{12}$	547
9.09	$2.46 \cdot 10^{10}$	173	3.70	$7.61 \cdot 10^{11}$	481
7.91	$3.70 \cdot 10^{10}$	194	3.72	$2.38 \cdot 10^{11}$	342
6.94	$2.82 \cdot 10^{10}$	181	3.86	$4.79 \cdot 10^{11}$	426
6.82	$1.34 \cdot 10^{11}$	283	2.46	$2.09 \cdot 10^{12}$	692
6.86	$9.93 \cdot 10^{10}$	258	2.95	$1.37 \cdot 10^{12}$	607
3.70	$7.58 \cdot 10^{11}$	494	3.30	$1.03 \cdot 10^{12}$	555
3.74	$5.01 \cdot 10^{11}$	433	2.87	$2.24 \cdot 10^{12}$	716
3.71	$2.53 \cdot 10^{11}$	345	2.31	$3.71 \cdot 10^{12}$	846
3.85	$1.30 \cdot 10^{11}$	288	2.79	$2.32 \cdot 10^{12}$	722
2.70	$1.88 \cdot 10^{12}$	661	2.40	$3.01 \cdot 10^{12}$	791

Table 1: Values of Nusselt, Rayleigh and Prandtl numbers obtained in the symmetric Smooth/Smooth case.

4 The asymmetric case: introduction of roughness elements

To destabilize the thermal and viscous boundary layers of the experiment, roughness elements are used on the hot/bottom plate, whereas the other one is kept smooth. This allows us to look for possible long distance influence of the roughness elements by checking the behavior of the cold/smooth plate.

4.1 Separation of plates

To compare our results to those of J.-C. Tisserand [2011], we shall separate our asymmetric cell into two half symmetric ones. This type of processing assumes independence of plates and, as we will see in section 4.2, this is indeed the case. The asymmetric cell with roughness on the bottom and without roughness on the top is sketched as case (a) of figure 5. We measure T_c , T_b and T_h . If we focus on the hot/rough plate and its corresponding half-cell, we can construct the symmetrical part by considering that, under Boussinesq approximation, the corresponding cold plate should be at the temperature $T_h - 2(T_h - T_b)$, case (b). This can be done for the cold plate too resulting in case (c).

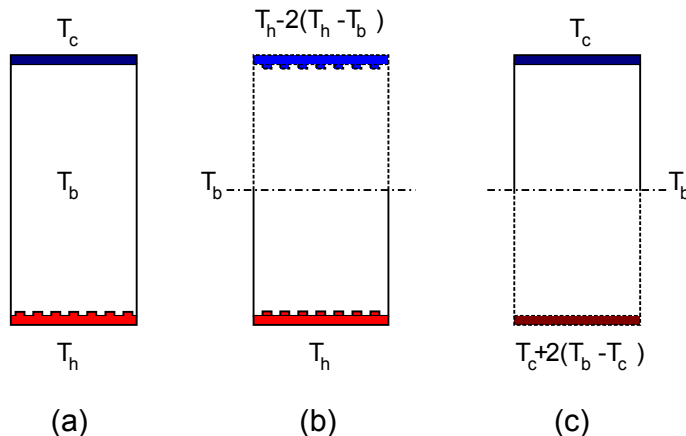


Figure 5: Separation of plates. (a) is the asymmetric cell we use, (b) is the symmetric cell based on the hot plate, (c) the symmetric cell based on the cold plate.

We then compute a difference of temperature corresponding to cases (b) and (c).

$$\Delta T_r = 2(T_h - T_b) \quad \Delta T_s = 2(T_b - T_c) \quad (9)$$

We also define and compute (Ra, Nu) couples for each cases.

$$Ra_r = \frac{\alpha g \Delta T_r H^3}{\nu \kappa}, \quad Nu_r = \frac{QH}{\lambda \Delta T_r}; \quad (10)$$

$$Ra_s = \frac{\alpha g \Delta T_s H^3}{\nu \kappa}, \quad Nu_s = \frac{QH}{\lambda \Delta T_s}. \quad (11)$$

This allow us to characterize the behavior of each plates separately.

4.2 Thermal transfer results

4.2.1 Cold/Smooth plate case

First, we focus on the cold/smooth plate. Indeed, J.-C. Tisserand [2011] showed that the thermal transfer of this plate is not modified by the presence of the roughness on the hot/rough plate. This is a good validation of the independence of plates. Indeed, if plates had not been independent, then, the roughness on the hot plate would have disrupted the cold plate. This still must be checked for the present 4 mm elements.

Figure 6 shows the (Nu_s, Ra_s) couple corresponding to the smooth/cold plate. Black open diamonds are the results obtained in the \mathcal{LC} classical smooth/smooth configuration described in section 3. The other open symbols correspond to J.-C. Tisserand [2011], triangles are for aspect ratio $\Gamma = 2.5$ and circles for aspect ratio $\Gamma = 1/2$, colors are Prandtl number series : blue for $T_b = 25^\circ\text{C}$, green for $T_b = 40^\circ\text{C}$ and brown for $T_b = 70^\circ\text{C}$ corresponding to a Prandtl number of 6.1, 4.3 and 2.5 respectively. Full symbols are the new results presented here, blue is for $T_b = 30^\circ\text{C}$, red for $T_b = 60^\circ\text{C}$. Note that the ordonates have been extended in order to range the same values than those of figure 7 for comparison. Focusing on each series, we can observe that they are qualitatively well aligned. Their mean values are always close to 1. The typical root mean square of those points is close to 5% with a maximal dispersion of order 10%.

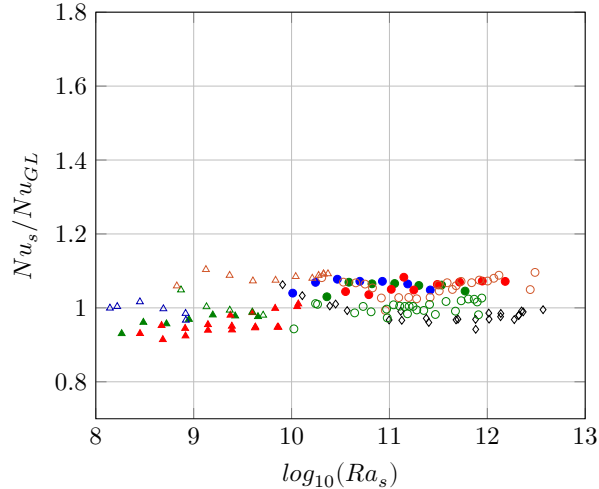


Figure 6: Thermal transfer of the smooth plate: Nu_s normalised by the Grossmann-Lohse model computed with respect to the experimental Prandtl number as a function of Ra_s . Colors refer to the bulk temperature T_b , blue is 25°C or 30°C , green is 40°C , red 60°C and brown 70°C . Open symbols refer to the $h_0 = 2$ mm of J.-C. Tisserand [2011], full symbols to the current $h_0 = 4$ mm elements. Triangles are for the \mathcal{SC} , circles for the large one \mathcal{LC} . Black diamonds are for the reference smooth/smooth cell presented in section 3.

We can conclude that the general behavior of the smooth/cold plate is not modified by the presence of roughness on the opposite hot plate whatever the case we examine here. They particularly remain in good agreement with the reference results obtained in the fully smooth cell. It claims for independence of plates, at first order, whatever the height of the roughness used on the other plate. Similar observations were also done by P. Wei [2014] when using asymmetrical cell. The behavior of the smooth plate was not changed by the introduction of roughness elements on the opposite plate. This was confirmed considering both top/smooth plate or bottom/smooth plate (ie: thermally regulated plate or constant heat flux plate). It suggests that the independence of plates is a robust result in the

range of Rayleigh number explored here (Ra larger than 10^8). Note that some recent Particle Image Velocimetry (PIV) measurements, O. Liot [2017], seem to show a major increase of the root mean square of the velocity close to the smooth plate respectively. This suggests that the smooth plate interacts with a modified bulk. However, the possible induced modifications of the thermal behavior of the smooth plate are smaller than the dispersion of our points.

Pr	Ra_s	Nu_s	Pr	Ra_s	Nu_s	Pr	Ra_s	Nu_s
5.32	$1.54 \cdot 10^{11}$	326	4.37	$2.00 \cdot 10^{11}$	353	2.98	$5.20 \cdot 10^{11}$	483
5.44	$8.47 \cdot 10^{10}$	272	4.37	$1.13 \cdot 10^{11}$	296	2.97	$3.08 \cdot 10^{11}$	407
5.45	$4.98 \cdot 10^{10}$	230	4.36	$6.63 \cdot 10^{10}$	250	2.98	$1.77 \cdot 10^{11}$	336
5.45	$2.94 \cdot 10^{10}$	196	4.37	$3.85 \cdot 10^{10}$	212	2.96	$1.04 \cdot 10^{11}$	285
5.46	$1.76 \cdot 10^{10}$	166	4.38	$2.29 \cdot 10^{10}$	174	2.96	$6.15 \cdot 10^{10}$	238
5.45	$1.03 \cdot 10^{10}$	136	4.35	$3.41 \cdot 10^{11}$	419	2.96	$3.56 \cdot 10^{10}$	202
5.36	$2.61 \cdot 10^{11}$	380	4.31	$5.93 \cdot 10^{11}$	492	2.94	$1.40 \cdot 10^{11}$	323
						2.96	$8.88 \cdot 10^{11}$	575
						2.96	$1.52 \cdot 10^{12}$	683

Table 2: Values for the smooth plate when using $h_0 = 4mm$ high roughness. Large cell.

Pr	Ra_s	Nu_s	Pr	Ra_s	Nu_s
4.36	$1.57 \cdot 10^9$	73	3.03	$2.37 \cdot 10^9$	82
4.37	$8.95 \cdot 10^8$	61	3.06	$3.99 \cdot 10^9$	97
4.37	$5.27 \cdot 10^8$	51	3.04	$6.80 \cdot 10^9$	116
4.38	$3.06 \cdot 10^8$	44	3.07	$1.14 \cdot 10^{10}$	136
4.39	$1.84 \cdot 10^8$	36	2.98	$1.17 \cdot 10^{10}$	139
4.40	$2.66 \cdot 10^9$	85	2.93	$7.34 \cdot 10^9$	112
4.40	$4.54 \cdot 10^9$	100	2.95	$4.27 \cdot 10^9$	95
			3.00	$2.46 \cdot 10^9$	81
			2.96	$1.40 \cdot 10^9$	68
			2.97	$8.18 \cdot 10^8$	58
			2.98	$4.84 \cdot 10^8$	48
			2.99	$7.19 \cdot 10^9$	112
			2.98	$4.23 \cdot 10^9$	95
			3.01	$2.46 \cdot 10^9$	80
			3.00	$1.40 \cdot 10^9$	67
			3.03	$8.25 \cdot 10^8$	57
			3.01	$4.70 \cdot 10^8$	49
			3.04	$2.83 \cdot 10^8$	41

Table 3: Values for the smooth plate when using $h_0 = 4mm$ high roughness. Small cell.

4.2.2 Hot/Rough plate case

Let us now focus on the rough/hot plate, ie. the (Nu_r, Ra_r) couple. The results are presented in figure 7 in the same normalised way as figure 6. The color and symbol choices are the same. The comparison between those two figures gives us another argument for the independence of plates. The general behavior of the rough/hot plate is different from the smooth/cold one.

As explained in J.-C. Tisserand [2011], the open symbols exhibit a transition when the height of the thermal boundary layer defined as $\delta_\theta = H/2Nu_r$ reaches the height of the roughness h_0 . This leads to an increase of the exponent a , expression 4.

The full symbols, corresponding to the new results obtained with $h_0 = 4mm$, exhibit another transition at high Rayleigh number both in the Large and the Small Cells. This transition can be interpreted as a saturation phenomenon. However, the range of Rayleigh number in the saturation part is too small to discuss a potential

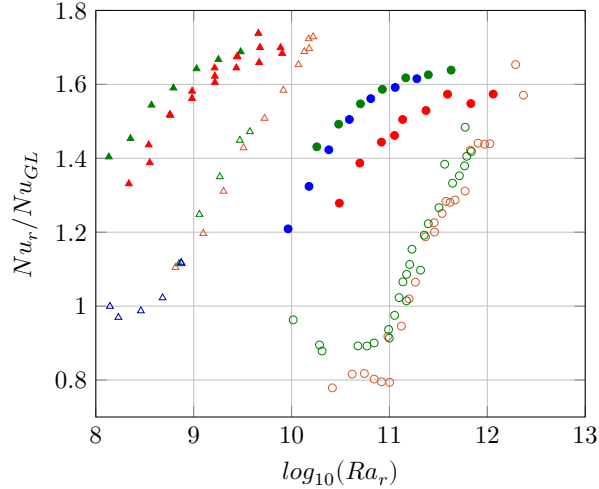


Figure 7: Thermal transfer of the rough plate: Nu_r normalised by the Grossmann-Lohse model computed with respect to the experimental Prandtl number as a function of Ra_r . Symbol and color choices are the same as figure 6.

exponent value. Comparison with other results obtained by different groups, in section 5, will allow a more detailed discussion on that point.

Pr	Ra _r	Nu _r	Pr	Ra _r	Nu _r	Pr	Ra _r	Nu _r
5.32	$1.15 \cdot 10^{11}$	444	4.37	$1.47 \cdot 10^{11}$	488	2.98	$3.92 \cdot 10^{11}$	650
5.44	$6.44 \cdot 10^{10}$	363	4.37	$8.47 \cdot 10^{10}$	403	2.97	$2.36 \cdot 10^{11}$	538
5.45	$3.90 \cdot 10^{10}$	299	4.36	$5.06 \cdot 10^{10}$	334	2.96	$1.36 \cdot 10^{11}$	444
5.45	$2.40 \cdot 10^{10}$	243	4.37	$3.03 \cdot 10^{10}$	274	2.96	$8.28 \cdot 10^{10}$	364
5.46	$1.51 \cdot 10^{10}$	196	4.38	$1.81 \cdot 10^{10}$	224	2.96	$4.98 \cdot 10^{10}$	298
5.45	$9.22 \cdot 10^9$	154	4.35	$2.50 \cdot 10^{11}$	581	2.96	$3.08 \cdot 10^{10}$	237
5.36	$1.91 \cdot 10^{11}$	530	4.31	$4.27 \cdot 10^{11}$	695	2.94	$1.13 \cdot 10^{11}$	406
						2.96	$6.78 \cdot 10^{11}$	761
						2.96	$1.15 \cdot 10^{12}$	916

Table 4: Values for the rough plate when using $h_0 = 4mm$ high roughness. Large cell. Precision of the measurement is $\pm 1.5\%$.

4.3 A characteristic length h_0

As the plates are independent, we can base the Rayleigh number on the height of the roughness and no longer on the height of the cell. This leads to the following normalisation of abscissa:

$$Ra_{h_0} = \left(\frac{2h_0}{H}\right)^3 Ra_r = \frac{\alpha g \Delta T_r (2h_0)^3}{\nu \kappa} \quad (12)$$

The prefactor 2 in $2h_0$ comes from symmetrised rough cell corresponding to the case (b) of figure 5. The results obtained with the normalisation are presented in figure 8. The collapse of all the different curves is good. We obtain a master curve which gives us a transition at low Ra_{h_0} , close to $Ra_{h_0} \approx 1.5 \cdot 10^4$, corresponding at the beginning of the thermal transfer enhancement when $\delta_\theta = h_0$. Then a saturation process appears at high Ra_{h_0} , close to 10^6 . This representation collapses the departure from the smooth-like behavior and the beginning of the saturation process.

In the saturated part of this curve, the thermal transfer enhancement exceeds 60%. We remind here that the presence of the roughness increase geometrically the surface of the hot plate of 40%. This leads us to an increase of the thermal transfer higher than a simple surface increase.

Pr	Ra _r	Nu _r	Pr	Ra _r	Nu _r
4.36	1.07 · 10 ⁹	108	3.03	1.65 · 10 ⁹	121
4.37	6.21 · 10 ⁸	89	3.06	2.73 · 10 ⁹	144
4.37	3.71 · 10 ⁸	74	3.04	4.66 · 10 ⁹	171
4.38	2.26 · 10 ⁸	60	3.07	7.71 · 10 ⁹	205
4.39	1.36 · 10 ⁸	50	2.98	8.02 · 10 ⁹	205
4.40	1.79 · 10 ⁹	128	2.93	4.76 · 10 ⁹	177
4.40	3.02 · 10 ⁹	152	2.95	2.80 · 10 ⁹	148
			3.00	1.64 · 10 ⁹	124
			2.96	9.63 · 10 ⁸	101
			2.97	5.77 · 10 ⁸	83
			2.98	3.47 · 10 ⁸	68
			2.99	4.58 · 10 ⁹	178
			2.98	2.77 · 10 ⁹	147
			3.01	1.65 · 10 ⁹	122
			3.00	9.61 · 10 ⁸	100
			3.03	5.72 · 10 ⁸	83
			3.01	3.56 · 10 ⁸	66
			3.04	2.18 · 10 ⁸	55

Table 5: Values for the rough plate when using $h_0 = 4mm$ high roughness. Small cell.

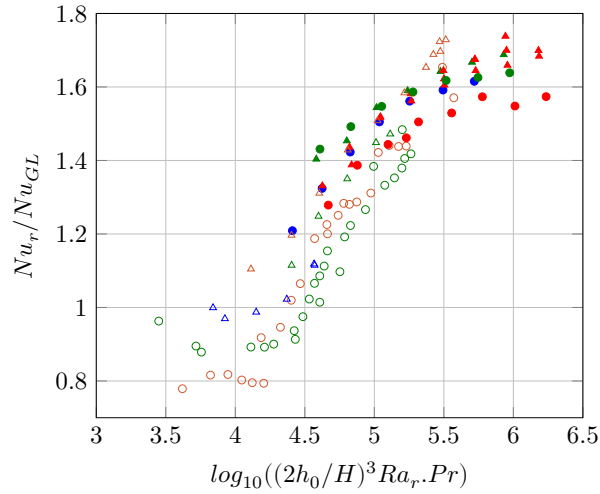


Figure 8: Thermal transfer of the rough plate case: Nu_r normalised by the Grossmann-Lohse model computed with respect to the experimental Prandtl number as a function of Ra_{h_0} . Symbol and color choices are the same as figure 6

5 Comparison with other roughness geometry

To compare our results to other, we will focus only on asymmetric cells. Indeed, as already mentioned, recent PIV measurements have shown that the asymmetry of the cell is also present in the flow characteristic. It is then reasonable to think that asymmetric and symmetric cells are not completely similar, even if common properties exist. P. Wei [2014] and J. Salort [2014] performed experiments in asymmetric cells, we will then use those points for comparison. The roughness used by Salort were similar to those used by J.-C. Tisserand [2011], square based roughness, 2 mm high, arranged in the same lattice as the one sketched in figure 2. The cell is a rectangular box with vertical aspect ratio $height/width = 1$ and horizontal aspect ratio $depth/width = 1/4$. The flow is quasi-2D in this experiment and exhibits a well-defined mean flow. A very confined geometry can significantly modify the thermal response of a cell, M. Kaczorowski [2014], including the local thermal transfer properties. The cell of Salort *et al*, in smooth/smooth configuration, exhibits a thermal behavior similar to those described in section 3. However, we cannot exclude that such confinement induces some differences using roughness. Wei and co-workers performed experiments in a cylinder of aspect ratio 1. They used pyramidal elements as roughness, sketched in figure 9. The base length d is equal to $2h_0$. The surface increase induced was of 41%. As both studies were also underlying an increase of the thermal transfer when the height of the thermal boundary layer was thinner than the roughness height, we can compare those points to the present ones in the spirit of section 4.3, see figure 10. Black symbols are for results of Wei *et al*, squares for Salort *et al*, colors correspond to different Prandtl number. The abscissa is the Rayleigh number based on the height of the roughness times the Prandtl number.

There is a large scattering between all different curves. However, considering that the roughness elements are different and the shape of the cell (some are cylinders, other rectangular based and quasi-2D), the general collapse can be considered as fair. We can extract some general thermal properties. Below a certain value, which corresponds to a thermal layer larger than the roughness height, the thermal transfer of the rough plate is consistent with a smooth one. Note that Nu_r/Nu_{GL} can be significantly lower than 1 for several experiments, J.-C. Tisserand [2011] and P. Wei [2014]. This is consistent with an extra thermal resistance induced by locked fluid between the roughness elements, see J.-C. Tisserand [2011].

At a nearly constant value, $Ra_{h_0}.Pr \approx 10^4$, a departure from the smooth-like behavior is observed. This part of the curves is consistent with a larger value of the exponent a of the so-called power law of the plate. The exponent value seems to be similar for those experiments except the gray squares, this particular point was discussed in J. Salort [2014]. They argue that the transition is due to a destabilization of the boundary layer induced by the interaction between layers and roughness elements. The destabilization can be total or partial leading to two potential behaviors. This destabilization of the boundary layer structure was, recently, confirmed by the work of O. Liot [2016] where, using PIV measurements in the boundary layer, they have found evidence of a turbulent velocity profile in that boundary. However, other enhancement mechanisms were also proposed in the past. In particular, Y.-B. Du [2000] used thermochromic liquid crystals to measure temperature fields close to a rough plate. Tips of roughness elements seemed to be preferential points of nucleation of thermal plumes. Following this hypothesis, we can assume that a cube can induce a higher increase of the thermal transfer than a pyramid since a cube is formed of four singularities interacting with the fluid whereas a pyramid is only exhibiting one singularity. Looking at figure 10, we note that between abscissa 4.2 and 6, the curves obtained with cubes are almost always above the ones obtained with pyramids, which is consistent with the previous assumption. Such an assumption suggests that a kind of density of singularities can be necessary to balance the Nusselt number. However, we have not found a satisfying criterion which allows a fairest collapse of the curves.

At larger Rayleigh number, $Ra_{h_0}.Pr > 10^6$, as already said, the solid circles and triangles are consistent with a saturation process. Black stars and +-circles, results of P. Wei [2014], allow to extrapolate the present results at larger Ra_{h_0} . They suggest that the normalised Nusselt number goes down to the value compatible with a simple surface increase (41% in that particular case). Note that, here again, the range of Rayleigh number explored is not sufficient to definitely conclude on that point. Still, this would be consistent with the idea that at a sufficiently high Rayleigh number, the boundary layers are small enough to allow the bulk to interact with the surface as it would with a smooth one. Moreover, a recent study, S. Toppaladoddi [2017], is focused on the influence of the density of roughness structures on the thermal transfer. To do so, they performed several 2D numerical simulations in a Rayleigh-Bénard system with roughness on both plates. They modified their roughness geometry to check the possible dependence of thermal transfer. Even if, we have excluded symmetric systems from our present analysis, this work has to be mentioned since it provides a possible saturation mechanism. Indeed, the authors define what they call a 'wavelength', $\lambda = \frac{d}{H}$, associated with roughness horizontal geometry. They report that the exponent of the Nusselt-Rayleigh relation depends on λ and that it exists an optimal value, λ_{opt} , at which a is maximum. Over λ_{opt} , a goes down to the typical value of the smooth case. Moreover, λ_{opt} is Rayleigh number dependent. We, then, can assume that the saturation can be associated with the overpassing of the optimal wavelength. To validate this

assumption, some experiments involving larger roughness elements would be necessary.

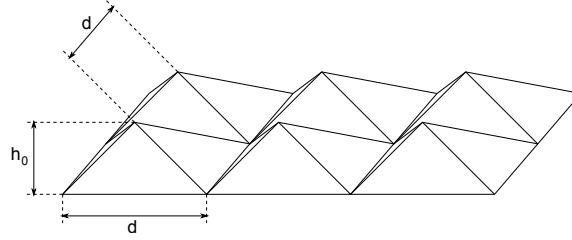


Figure 9: Sketch of the pyramidal roughness used by P. Wei [2014].

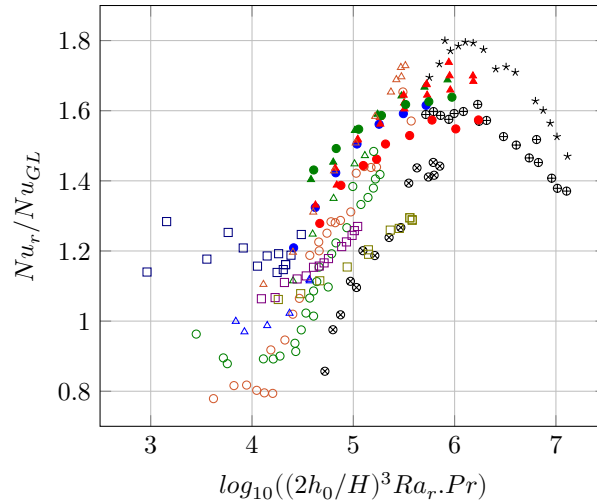


Figure 10: Same representation as figure 8. Other asymmetrical experiments are added for comparison. Full circles: \mathcal{LC} $h_0 = 4mm$, full triangles: \mathcal{SC} $h_0 = 4mm$, open circles: Tisserand *et al.*: \mathcal{LC} , open triangles: Tisserand *et al.*: \mathcal{SC} . Black stars: Wei *et al* $h_0 = 8mm$ R/S, black +-circles: Wei *et al* $h_0 = 8mm$ S/R, black x-circles: Wei *et al* $h_0 = 3mm$ R/S. Squares: Rectangular Cell: Salort *et al.*

6 Conclusion

We report, in this article, some new thermal transfer measurements in a cylindrical Rayleigh-Bénard cell with square roughness on the hot/bottom plate for two different cell aspect ratios. We compare obtained results to previous studies led with different roughness shape and/or dimensions. The well-known Grossmann-Lohse law is used as a reference for the smooth case thermal transfer. We distinguish three main kinds of thermal transfer behavior in presence of roughness. The first one, when the thermal boundary layer is thicker than the typical roughness height, is similar to the thermal transfer with a smooth plate. The efficiency of the thermal transfer can be reduced compared to the smooth case which can be due to a larger impedance of the boundary layer between the roughness. When the boundary layer thickness gets down to the roughness height, a second thermal transfer behavior appears. We observe an increase of the so-called power law describing the relation of the Nusselt versus Rayleigh numbers. The thermal transfer becomes larger than a simple surface increase due to roughness elements. This is consistent

with the changes of the thermal and viscous boundary layers structure observed in previous studies (J. Salort [2014], O. Liot [2016]) which imply an intrinsic thermal flux enhancement. Finally, for larger Rayleigh numbers, a third behavior is characterized by a reduction of the thermal transfer enhancement. The Nusselt number seems to go back to the smooth one corrected by the surface increase due to the roughness. To confirm this assumption, some experiments at higher Rayleigh numbers should be performed.

We have shown that both plates are independent relatively to the thermal transfer. The use of a Rayleigh number based on the roughness height, instead of the cell one, leads to a fair collapse of the thermal transfer curves for different roughness shape and/or elements even if a dispersion (possibly due to the shape differences or the cell aspect ratio) is still present. Some work remains necessary to understand the balance of the two probable main thermal transfer enhancement processes (boundary layers destabilization and plume emission increase). Other roughness shapes with more or less geometrical singularities could be interesting. Finally, to propose a better master curve of the thermal transfer, some additional experiments are also required specially to check the influence of the spatial distribution, or density, of roughness elements.

ACKNOWLEDGMENTS

We highly thank Marc Moulin for technical assistance. We also want to thank Anne Sergent and Bérengère Podvin for usefull discussions on this subject. This work has been supported by the Région Rhône-Alpes (Cible 2011, n°2770).

References

- G. Ahlers. Effect of sidewall conductance on heat-transport measurements for turbulent Rayleigh-Bénard convection. *Phys. Rev. E*, 63, 2000.
- J. Schumacher F. Chillà. New perspectives in turbulent Rayleigh-Bénard convection. *Eur. Phys. J. E*, 35, 2012.
- et al* G. Ahlers. Non-Oberbeck-Boussinesq effects in strongly turbulent Rayleigh-Bénard convection. *J. Fluid Mech.*, 569, 2006.
- et al* J.-C. Tisserand. Comparison between rough and smooth plates within the same Rayleigh-Bénard cell. *Phys. Fluids*, 23, 2011.
- et al* J. Salort. Thermal boundary layer near roughnesses in turbulent Rayleigh-Bénard convection: flow structure and multistability. *Phys. Fluids*, 26, 2014.
- et al* J.J. Niemela. Turbulent convection at very high Rayleigh numbers. *Nature*, 404, 2000.
- K.-Q. Xia M. Kaczorowski, K.-L. Chong. Turbulent flow in the bulk of Rayleigh-Bénard convection: aspect-ratio dependence of the small-scale properties. *J. Fluid. Mech*, 747, 2014.
- et al* O. Liot. Boundary layer structure in a rough Rayleigh-Bénard cell filled with air. *J. Fluid Mech.*, 786, 2016.
- et al* O. Liot. Large scale circulation and boundary layer structure in a rough Rayleigh-Bénard cell filled with water. *under consideration for publication in Phys. Rev. Fluid*, 2017.
- et al* P.-E. Roche. Observation of the 1/2 power law in Rayleigh-Bénard convection. *Phys. rev. E*, 63, 2001a.
- et al* P.-E. Roche. Side wall effects in Rayleigh-Bénard experiments. *Eur. Phys. J. B*, 24, 2001b.
- L.Skrbek P. Urban, V. Musilova. Efficiency of heat transfer in turbulent Rayleigh-Bénard convection. *Phys. Rev. Lett.*, 107, 2011.
- et al* P. Wei. Heat transport properties of plates with smooth and rough surfaces in turbulent thermal convection. *J. Fluid Mech.*, 740, 2014.
- et al* R. J. A. M. Stevens. The unifying theory of scaling in thermal convection: the updated prefactors. *J. Fluid Mech.*, 730, 2013.
- C. Laroche S. Ciliberto. Random roughness of boundary increases the turbulent convection scaling exponent. *Phys. Rev. Lett.*, 82, 1999.

- D. Lohse S. Grossmann. Scaling in thermal convection: a unifying theory. *Jour. Fluid Mech.*, 407, 2000.
- J. S. Wettlaufer S. Toppaladoddi, S. Succi. Roughness as a route to the ultimate regime of thermal convection. *Phys. Rev. Lett.*, 118, 2017.
- et al* X. Chavanne. Turbulent Rayleigh–Bénard convection in gaseous and liquid He. *Phys.of Fluids*, 13, 2001.
- P. Tong X.-L. Qiu, K.-Q. Xia. Experimental study of velocity boundary layer near a rough conducting surface in turbulent natural convection. *J. of Turb.*, 6, 2005.
- P. Tong Y.-B. Du. Enhanced heat transport in turbulent convection over rough surface. *Phys. Rev. Lett.*, 81, 1998.
- P. Tong Y.-B. Du. Turbulent thermal convection in a cell with ordered rough boundaries. *J. Fluid Mech.*, 407, 2000.